IOPscience

Manuscript version: Accepted Manuscript

The "**Accepted Manuscript**" is the author's original version of an article including any changes made following the peer review process but excluding any editing, typesetting or other changes made by IOP Publishing and/or its licensors.

During the embargo period (the 12 month period from publication of the Version of Record of this article), the Accepted Manuscript:

- is fully protected by copyright and can only be accessed by subscribers to the journal;
- cannot be reused or reposted elsewhere by anyone unless an exception to this policy has been agreed in writing with IOP Publishing

As the Version of Record of this article is going to be/has been published on a subscription basis, this Accepted Manuscript will be available for reuse under a CC BY-NC-ND 3.0 licence after a 12 month embargo period.

After the embargo period, everyone is permitted to copy and redistribute this article for Non-Commercial purposes only, provided they*:

- give appropriate credit and provide the appropriate copyright notice;
- show that this article is published under a CC BY-NC-ND 3.0 licence;
- provide a link to the CC BY-NC-ND 3.0 licence;
- provide a link to the Version of Record;
- do not use this article for commercial advantage or monetary compensation; and
- only use this article in its entirety and do not make derivatives from it.

*Please see CC BY-NC-ND 3.0 licence for full terms.

View the Version of Record for this article online at iopscience.org

This content was downloaded from IOPscience

Metallographic autopsies of full-scale ITER prototype Cable-in-Conduit Conductors after full cyclic testing in SULTAN:

2. Significant Reduction of Strand Movement and Strand Damage in Short Twist Pitch CICCs

Carlos Sanabria [1], Peter J. Lee [1], William Starch [1], Arnaud Devred [2], and David C. Larbalestier [1]

[1] Applied Superconductivity Center, National High Magnetic Field Laboratory, Florida State University, Tallahassee, FL 32310, USA.
[2] ITER Organization, Building 72/4046, TED, Magnet Division Route de Vinon-sur-Verdon - CS 90 046 - 13067 St Paul Lez Durance Cedex - France.

Abstract

Prototype cable-in-conduit-conductors (CICCs) destined for use in the Toroidal Field (TF) and Central Solenoid (CS) coils of the ITER experimental fusion reactor underwent severe cyclic loading in the SULTAN facility. Their autopsies revealed significant and permanent transverse strand migration due to the large Lorentz forces of the SULTAN test. The movement resulted in a 3-7% void fraction increase on the Low Pressure (LP) side of the longer twist pitch CICCs. However, short twist pitch conductors exhibited less than 1% void fraction increase in the LP side, as well as a complete absence of the Nb_3Sn filament fractures observed in the longer twist pitch conductors. We report here a detailed strand-to-cable analysis of short and longer "baseline" twist pitch CICCs. It was found that the use of Internal Tin strands in the longer "baseline" twist pitch CICCs can be beneficial possibly because of their superior stiffness—which better resist strand movement—while the use of Bronze Process strands showed more movement and poorer cyclic test performance. This was not the case for the short twist pitch CICC. Such conductor design seems to work well with both strand types. But it was found that despite the absence of filament fractures, the short twist pitch CICC made from the Internal Tin strands studied here developed severe strand distortion during cabling which resulted in diffusion barrier breaks and Sn contamination of the Cu stabilizer during the heat treatment. Conversely, the short twist pitch CICC made from Bronze Process strands preserved diffusion barrier integrity.

I. Introduction

The high magnetic fields and the cyclic operation of the ITER Toroidal Field (TF) and Central Solenoid (CS) coils are a difficult challenge for brittle Nb_3Sn—the superconductor of choice in this field range. To guarantee their performance, short, full-scale cable-in-conduit conductors (CICC) have been rigorously tested in the SULTAN facility to make sure that they can withstand cyclic loading over the planned lifetime of ITER. Qualification of the Toroidal Field (TF) conductor design was completed in 2010 [1] and although some degradation of their current sharing temperature, T_{cs}, was observed, sufficient T_{cs} performance was retained to predict a full lifetime of the TF coils. However, the CS coils are required to withstand many more cycles; and because initial testing showed continuous T_{cs} degradation over 10,000 cycles, it was concluded that improvements in CS cable performance were necessary [2], [3]. At this point, a comprehensive R&D program was launched [4] with the purpose of finding a conductor design that would withstand the 60,000 cycles expected for the CS magnet system [5]. To achieve this, several different CS prototype conductors were tested at the SULTAN facility where ITER-coil operating conditions can be simulated on 3 m long straight samples. Throughout the

qualification test, the change in current sharing temperature, ΔT_{cs} [6], is monitored (which is a very accurate assessment of the evolution in the conductor's quality during the test). The main goal was to evaluate the effect of varying important CICC design parameters such as void fraction, twist pitch length, triplet configuration and strand type with the aim of finding a conductor that would show a stable T_{cs} after a satisfactory number of cycles [4]. The program concluded with surprisingly good results for short twist pitch CICC designs, exhibiting no T_{cs} degradation under electromagnetic (EM) cycling, and instead a slight T_{cs} increase [7]. Multiple studies were carried out to better understand these results, including finite element analysis [8] and strain measurements supported by magnetic susceptibility [9]. Such multiple characterizations have been vital to unravelling the properties of these remarkably complex conductors—in which all conductor parameters play relevant roles but their collective effect is what determines the performance.

Here we describe post-mortem analyses [10] on several of these SULTAN-tested samples. Our experiments were designed to understand the mechanical effects of the Lorentz force acting on the CICC using digital microscopy to quantify changes in the CICC components after SULTAN testing—especially any which could be sources of irreversible degradation. Among such testing effects are permanent *transverse strand movement* which alters the local stress state and produces variations in the reversible (*i.e.* elastic) strain-sensitive superconducting properties of the Nb_3Sn [11]. In some cases we found *filament fractures* indicative of local high tensile stress concentrations. Our previous studies have shown that Nb_3Sn fractures occur most often when the strands undergo severe bending [12] but it is also known that significant degradation of strand current-carrying capability can occur reversibly, even without filament fracture [13]. A key aspect of the driving argument for the short twist pitch was that it would reduce the distance between strand contact points, better lock the strands into place, and prevent both elastic and plastic damage—including fracture of the brittle Nb_3Sn. The short twist pitch was a success in ITER conductors, but it is interesting to see that previous attempts of short twist pitch in smaller CICCs led to a lower performance [14].

A CS CICC contains 576 fully transposed strands, built up in five cabling stages. The final six sub-cable bundles ("petals") are twisted around a central helical spacer that acts as a cooling channel. The cable is drawn into a stainless steel jacket [4], [15], as shown in Figure 1, and then compressed to final dimensions [7].

Because of the brittle nature of Nb_3Sn, the superconducting wires must be manufactured using ductile precursors—bronze and Nb for *Bronze Process* strands and Sn, Cu and Nb for *Internal Tin* strands, which are reacted to form Nb_3Sn only after insertion of the cable into its jacket.

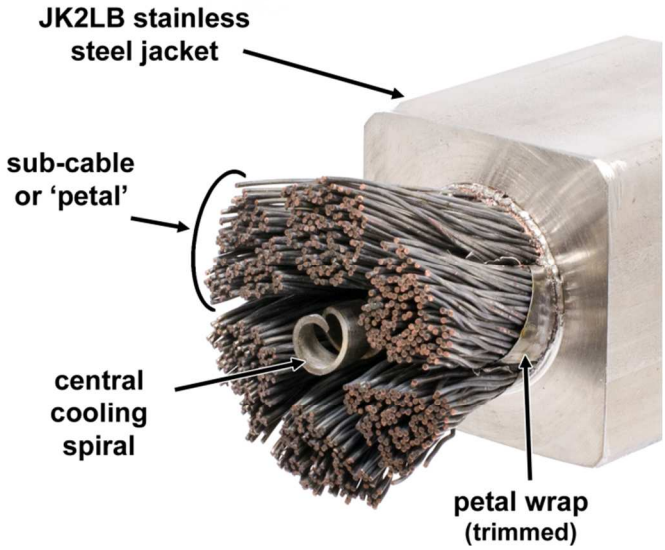

Figure 1. Photograph of a CS prototype CICC after partial removal of the stainless steel jacket and stainless steel wraps around the 6 petals. The 576 strands and the central helium flow tube are evident, as is the thick stainless steel jacket.

For conductor qualification, 3 m-long straight sections of different CS prototype conductors were prepared and reacted under the supervision of the ITER domestic agencies (DA). A SULTAN tests consists of a series of

electromagnetic cycles and occasional warm-up cool-down cycles in which T_{cs} change is monitored. More detailed descriptions of the results of the SULTAN testing can be found in [4].

This paper shows metallographic deconstruction and analysis of *four* different R&D prototype conductors, of which two (CSJA2-2 and CSIO1-2) use the longer *baseline* twist pitch, while the other two (CSJA3-1 and CSIO2-2) use the *short* twist pitch alternative. Additionally, two of them rely on *Bronze Process* (BR) wires and the other two rely on the *Internal Tin* (IT). For simplicity we designate these as Baseline-BR, Baseline-IT, Short-BR and Short-IT. Their relevant parameters are shown in Table 1, together with the void fraction measured after testing by our digital imaging techniques [10].

Table 1 Measured conductor parameters for the conductor prototypes analyzed

Formal name	Name for this article	ΔT_{cs}, K	Cycles	ΔT_{cs} (6000 cycles, K)	Triplet Configuration	Twist Pitch	Void Fraction after Test
CSJA 2-2	Baseline-BR	-1.36	17,000	-0.43	2 x sc + 1 Cu	45/84/145/251/453	35.5 ± 0.38%
CSIO 1-2	Baseline-IT	-0.42	11,200	-0.22	2 x sc + 1 Cu	45/85/147/248/424	34.0 ± 0.30%
CSIO 2-2	Short-IT	0.20	6,100	0.21	2 x sc + 1 Cu	22/45/81/159/443	31.0 ± 0.40%
CSJA 3-1	Short-BR	0.29	8,650	0.26	2 x sc + 1 Cu	22/45/81/159/443	32.9 ± 0.60%

The T_{cs} evolution of each CICC is compared in Figure 2, which also shows the warm-up cool-down (WUCD) cycles used to simulate instances in which the ITER machine would be brought to room temperature and back to operational temperature. These WUCD cycles were inserted at varying cycle numbers due to scheduling constraints [4]. The most relevant result in Table 1 and Figure 2 is the slight increase in T_{cs} as a function of electromagnetic (EM) cycles for short twist pitch *and* conversely its decrease for baseline twist pitch samples. The results of this article intend to explain the mechanism by which these two diverging behaviors take place.

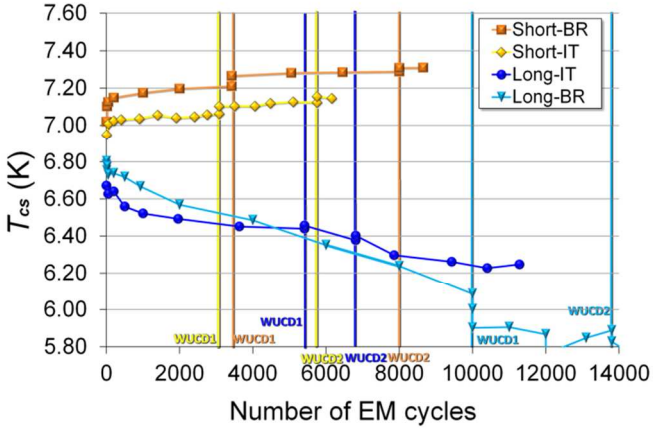

Figure 2. Normalized T_{cs} versus number of electromagnetic loading (EM) cycles of the conductors studied here. The normalization is done with respect to the T_{cs} measured on the first cycle.

II. Experimental Procedures

A. Introduction

Because the deconstruction techniques presented here are not always conventional, we spend time establishing our concepts and approaches. Some of these were introduced thoroughly in [10] and will only be refreshed here while others are new to this second study and will be explained in more detail.

B. Glossary from previous CICC metallographic studies

During the electromagnetic (**EM**) and **warm-up cool-down** cycling of the CICCs (*i.e.* the SULTAN test), strand movement is possible inside the conduit. Therefore under the influence of the Lorentz force the strands migrate and pile up on the **High Pressure (HP) side** of the conductor producing a void fraction reduction there, and an opposing void expansion on the **Low Pressure (LP) side**. Because these conductors are fully transposed, the 6 **petals** (sub-cables) periodically rotate between the HP and LP sides along the conductor. So, in order to effectively identify the petal location, we define their angular position with respect to the Lorentz force, defining 0° as the direction of the Lorentz force. 0° thus defines the HP side, while the LP side is located at 180°. The range of void fraction values across the 6 sub-cables is of great interest because a large void fraction is known to degrade the performance of the CICC [8], [16]. We use the **petal void fraction deviation** (from the average) to report either a reduction (negative value) or expansion of the void fraction (positive value). To measure the void fraction we used high resolution **transverse cross section images** taken with a laser scanning confocal microscope (LSCM) stitched together to produce high magnification images of more than 200 Megapixels. All key components of the CICC (void, strands, conduit, etc.) are then isolated and measured using common techniques and procedures from the widely used open-source software package, Fiji [17] (based on ImageJ [18]). Such image can also be used to track the center of mass of each strand in relation to the conduit center and therefore an **average strand center of mass offset** can be calculated.

Longitudinal sections of extracted strands are also valuable. For example, identification of cold work in the Cu sheaths of superconducting strands can indicate significant pinch points at **cross-overs** where there is enough stress produced during SULTAN testing to plastically deform the annealed Cu of the strands after Nb_3Sn reaction. In extreme but rare cases, filament fracture can occur near these contact points [10]. Another example is the observation of filament fractures produced from bending of the strands during SULTAN test. In previous studies we have found that strand sections with higher **curvature** (the local curvature is defined during cabling) are more prone to filament fractures [10], [12]. Therefore, when extracting strands for metallographic analysis, we selected two groups, one that we call "bent" and one that we call "straight" (the tails of the strand curvature Gaussian distribution [10]). Those considered bent and straight have curvatures lower than 0.95 or higher than 0.98, where 1 is a perfectly straight strand piece.

A final point concerns the location of the conductor segments taken for metallography. Along the three meters of a SULTAN sample only about 420 mm lie in the 10.8 T peak field that defines the test, therefore conductor segments from this high field zone (**HFZ**) are of most interest and are the main point of discussion here. Additionally comparison with the low field zone (**LFZ**) serves as control since the Lorentz force during testing is significantly lower in this region of magnetic field lower than 1 T.

C. Deconstruction procedures used here and previously

A diamond saw cut was used to extract ~400 mm long samples, from which Electrical Discharge Machining (EDM) sectioned smaller 150 mm long samples from both the HFZ and LFZ of the SULTAN samples. We also wanted two pieces from each zone, one for *strand extraction* and one for *transverse cross sectional imaging*, thus requiring four 150 mm long pieces per CICC. Segments assigned for strand extraction were stripped from their steel jackets using an end mill and then submerged in a 20% HCl solution to remove the Cr plate. Segments assigned for transverse cross section analysis were vacuum epoxy impregnated and then further cut to enable three cross sections per sample.

D. Additional procedures for the SULTAN samples described here

During deconstruction of the short twist pitch conductors (Short-BR and Short-IT), we observed that the strands were heavily sintered together and interlocked, making it very difficult to extract individual strands without damaging them. To overcome the tight twist, the cable (which was quite rigid, even without the jacket) was cut further using EDM to get a ~12 mm long piece, as shown in Figure 3. These pieces were then submerged in a 20% HCl bath for Cr plate removal. In this case, the etch time needed to be for much longer to overcome the severe sintering of the strands (24 as opposed to 2 hours in [10]). Removing the Cr plate was sufficient to release the strands without damage.

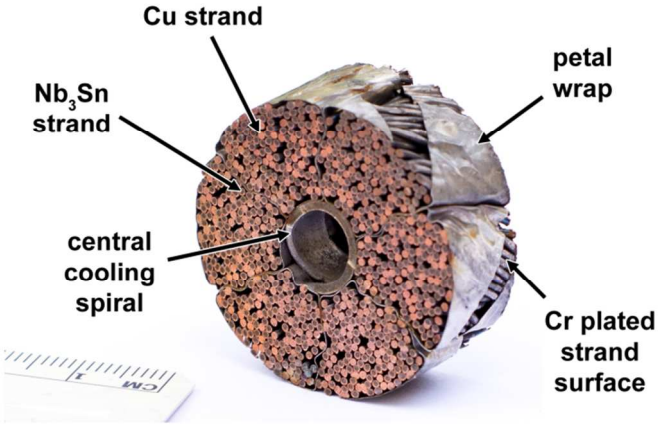

Figure 3. Photograph of one of the short pieces used to extract strands from the short twist pitch samples. This piece was submerged in a 20% HCl bath for 24 hours to remove the Cr, which allowed separation of the strands with very little force.

E. Additional measurements

The circular distortion of the non-Cu area of each strand was also calculated for these 4 CICCs. This required transverse cross sectional images like those used for void fraction measurements but in this case the CICC cross sections were submerged for 7 minutes in a 50% HNO_3 solution prior to LSCM imaging in order to etch back the copper strands and the Cu-jacket of the Nb_3Sn composite strands. This facilitates the isolation and measurement of the non-Cu areas of each strand (Figure 4). Once the images were translated into binary images (Figure 4c), the "roundness" of the strand cross-sections was defined by the formula:

$$R = \frac{4 \cdot A}{\pi \cdot {M_A}^2} \quad (1)$$

where A is the area of the feature, M_A is the major axis and R is the roundness (unity for a perfect circle). An example of the roundness evaluations is shown in (Figure 4d) where the lightest color (yellow) corresponds to a perfect circle and the darkest color (indigo) corresponds to an ellipse with roundness of 0.4.

There are two features that can affect the measurement of R: One is the angle in which the strand is being cut by the transverse cross section—this is a function of the twist pitch. While the second is produced by distortions induced during cabling and compaction of the conductor. Unfortunately former cannot be factored out in a reliable manner, but as it will become apparent its effect is much lower than that of the former.

III. Results

A. Transverse cross section analysis of SULTAN tested CICCs

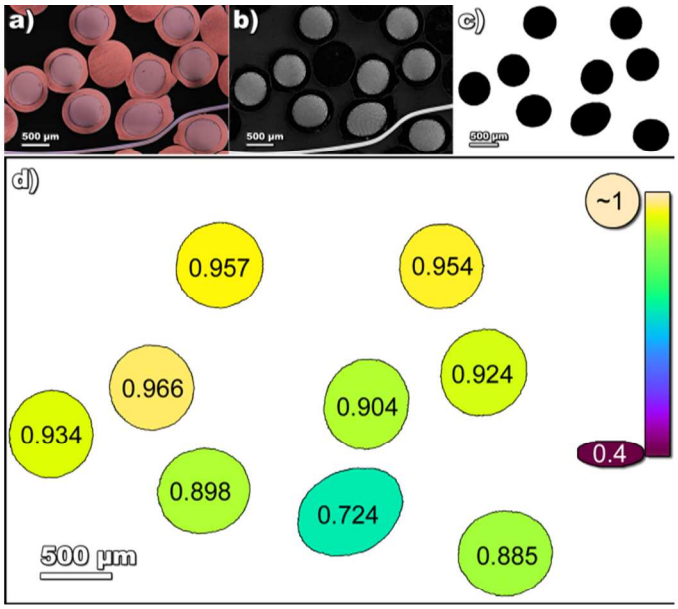

Figure 4. SLCM image of a group of strands (a) before etching and (b) after etching. (c) Binary images of the non-copper areas and (d) color/intensity-coded non-Cu roundness map (darker = more distorted).

The whole-conductor void fractions (excluding the central helix but including the void regions lying between the conduit and the petal wrap) of each CICC averaged from six different transverse cross sections along the length are shown in Table 1. These fractions vary from a high of 35.5% (Baseline-BR) to a low of 31.0% (Short-IT). However, these numbers vary strongly from petal to petal in the HFZ samples, depending on the petal orientation to the Lorentz force. The *petal void fraction deviation from the average* (see glossary above) is shown in Figure 5. Two key results are immediately obvious: first, as expected, there is almost no variation in the LFZ samples, and second, there is a much higher void fraction redistribution in the longer, baseline twist pitch samples than in the short twist pitch samples (up to 14% compared to only 2-3%).

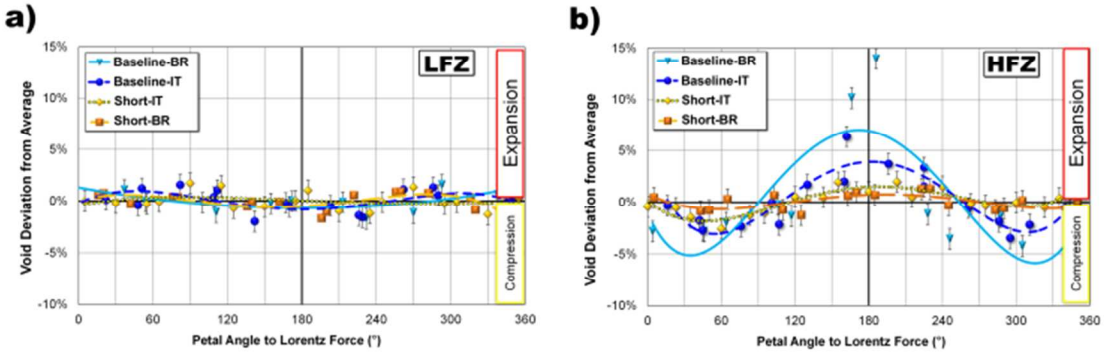

Figure 5. Petal void fraction deviation from the global average as a function of petal orientation with respect to the Lorentz force for (a) the LFZ and (b) the HFZ sample of each conductor. Petals in the vicinity of 180° are on the LP side. The trend lines are fourth order polynomial fits to guide the eye.

Figure 6 shows the *average strand center of mass offset* (see glossary above) with respect to the conductor center of several cross sections from each CICC. It can clearly be seen that the offset in the short twist pitch conductors is much lower than for the longer, baseline twist pitch conductors. In fact the offset in short twist pitch conductors is almost the same amount in both the HFZ and the LFZ, leading one to believe there was negligible movement. However, the strand offset in *all* HFZ cross sections of all samples is always in the direction of the Lorentz Force while it is random in the LFZ sections. The scalar values for each conductor (averaged from

Figure 6) are shown in Figure 7 to illustrate further the large differences in strand movement.

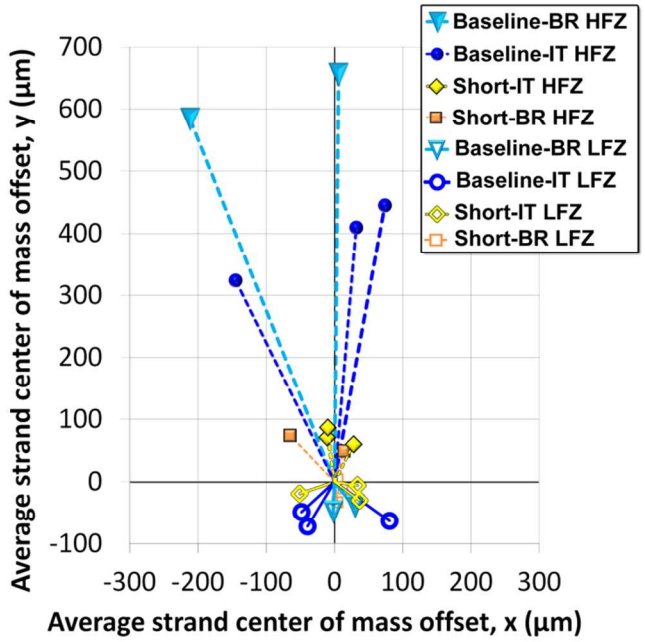

Figure 6. Average strand center of mass offset. The offset of strands in the HFZ is along a vector that lies within ± 30° of the Lorentz force direction in all samples while in the LFZ the offset is completely random

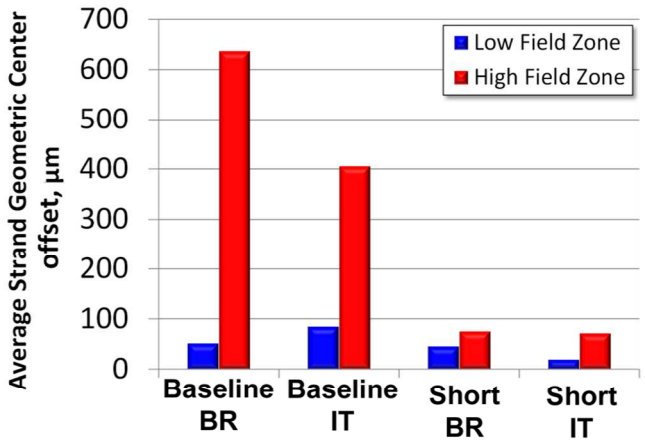

Figure 7. Scalar values of the average strand center of mass offset values in Figure 6 for each conductor.

The much larger strand offset of the Baseline-BR (~ 620 µm) compared to the Baseline-IT (~ 400 µm) conductors is consistent with the lower stiffness of the reacted bronze compared to the reacted Internal Tin strands [13]. Lower overall conductor stiffness allows more strand movement within the petal, a greater void fraction redistribution [19] and (as will be seen in the next sub-section) more frequent filament fracture. The movement observed for the short twist pitch conductors is dramatically lower because the strands are effectively locked together—hence their collective stiffness increased. There is still, however, detectably more strand displacement in the HFZ than the LFZ samples of these short twist pitch conductors. Considering that there was insufficient strand-strand movement to break the sintered bond produced during the reaction HT, their offset may no longer be that of individual, unsupported strand lengths between two contact points (as modeled in [20] and seen in [10] and [12]), but rather a more collective movement involving multiple strands or even whole conductor petals within the jacket.

The roundness values of the non-copper areas, which are consequences of the deformation during cabling and compaction of the strands, are color coded for a single LFZ cross section from each sample in Figure 8. The most striking result is the severe distortion that the Short-IT undergoes when cabled. Notice that in all cases, the outermost strands are the most distorted, suggesting that the final compaction has a strong impact on the strands near the stainless steel jacket.

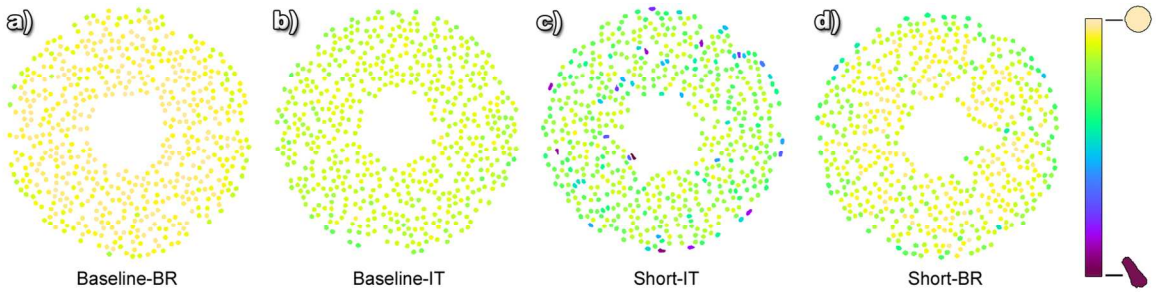

Figure 8. Color/intensity coded roundness (darker = more distorted) obtained from the non-copper areas of a single cross section of (a) Baseline-BR, (b) Baseline-IT, (c) Short-IT, and (d) Short-BR.

Using the strand roundness values in Figure 8, frequency distribution curves were generated to illustrate further the differences in strand distortions between the cables (Figure 9). It can be appreciated that the reduction in "roundness" is quite severe for the Short-IT sample.

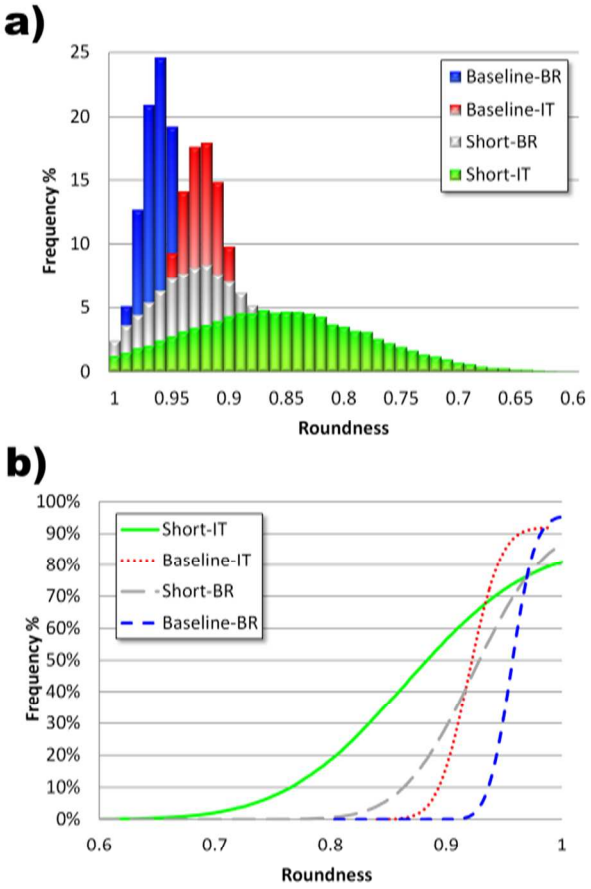

Figure 9. (a) Roundness distribution and (b) cumulative distribution plot generated with the statistical values from the cross sections in Figure 8.

Investigating the strand distortion in the Short-IT sample in more detail, it was observed that on average a conductor cross section would have 14 strands with a broken diffusion barrier, all of which had roundness values lower than 0.73. Additionally it was found that these 14 broken barriers represented 43% of all the strands with roundness values lower than 0.73. Then, using this limit of 0.73 to calculate the normal probability distribution from Figure 9 (simple Gaussian distribution calculations), we found that the probability of finding a strand with a roundness lower than 0.73 is 6.46% and since 43% of those often present broken barriers, the probability of finding a broken barrier is 2.78%. There were no broken diffusion barriers found in the other samples in this

article.

Stabilizer copper poisoning around broken barriers was studied further using Energy Dispersive Spectroscopy (EDS) performed at 15 kV using standardless analysis (EDAX TEAM V3-4) with an EDAX Apollo XP SDD detector. Figure 10 shows point EDS measurements in the copper for a highly deformed strand in a LFZ cross-section from the Short-IT sample. Tin contents for these points are shown in Table 2.

There are three points in the stabilization copper of this strand where the tin contents are higher than 0.1 at % Sn and it is known from [21] that at this concentration the RRR can be as low as ~20. Note also in Figure 10 that the IT strand cross-section is heavily distorted compared to the pure Cu stabilizer strand that is in contact with it to its left.

Figure 11 shows EDS spot measurements on one of the most distorted cases found in the Short-BR sample (also a HFZ cross section), but in this case, no tin signals were found at any point in the Cu. Figure 11 also shows evidence of cold work in the Cu stabilizer, as evidenced by micro-misorientations in this back-scattered electron image of the Cu. These are a result of the Lorentz force acting at that particular contact point, however, notice that the cold work does not appear inside the diffusion barrier unlike the Baseline-BR sample (this will be discussed further below) and that there is no evidence of filament damage, unlike the conductors studied in [10].

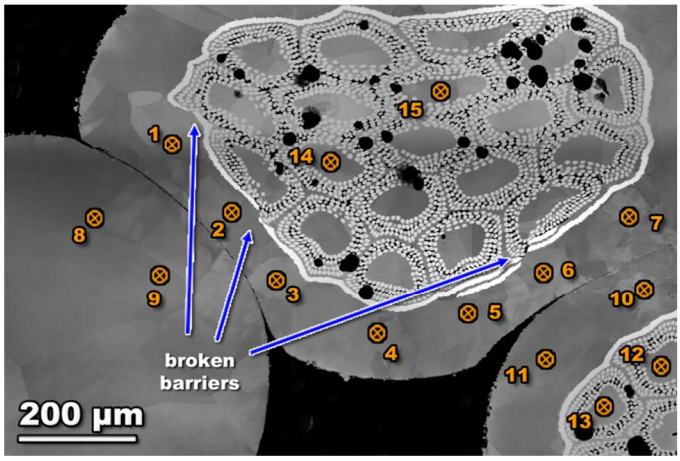

Figure 10. FESEM standardless EDS point measurements of local Sn and Cu content around a broken barrier in the LFZ of the Short-IT sample. Black dots are stains from polishing fluid.

Table 2. Standardless EDS point measurements of local Sn and Cu content for locations in Figure 10

Position	Location	Cu-at%Sn
1	**Cu stabilizer**	**0.21 ± 0.04**
2	**Cu stabilizer**	**1.11 ± 0.04**
3	**Cu stabilizer**	0.04 ± 0.02
4	**Cu stabilizer**	0.00 ± 0.00
5	**Cu stabilizer**	0.07 ± 0.03
6	**Cu stabilizer**	**0.60 ± 0.05**
7	**Cu stabilizer**	0.01 ± 0.01
8	Cu strand	0.00 ± 0.00
9	Cu strand	0.01 ± 0.01
10	**Cu stabilizer**	0.00 ± 0.00
11	**Cu stabilizer**	0.00 ± 0.00
12	Interior Cu(Sn)	5.14 ± 0.12
13	Interior Cu(Sn)	5.49 ± 0.12
14	Interior Cu(Sn)	6.36 ± 0.13
15	Interior Cu(Sn)	6.52 ± 0.14

B. *Strand extraction*

Our first observation after we removed the jackets was that the strands were fully sintered together in both the HFZ and the LFZ of the short twist pitch samples, suggesting that the forces exerted during SULTAN testing were not sufficient to break this bond. The baseline twist pitch samples on the other hand, had no sintering in the HFZ while significant sintering was evident in the LFZ, suggesting that strand movement (seen in Figure 5 and Figure 6) broke any bonding present in the HFZ of these baseline twist pitch samples.

The filament fracture analysis showed that none of the conductors whose strands remained sintered produced filament fractures; this includes the short twist pitch samples in their entirety and the low field zones of every sample. Just as in [10] we can conclude that the axial compression produced during cool-down in SULTAN is not high enough to produce fracture strains, despite the overall average compression approximated between 0.5% and 0.3% [9], [16], [20].

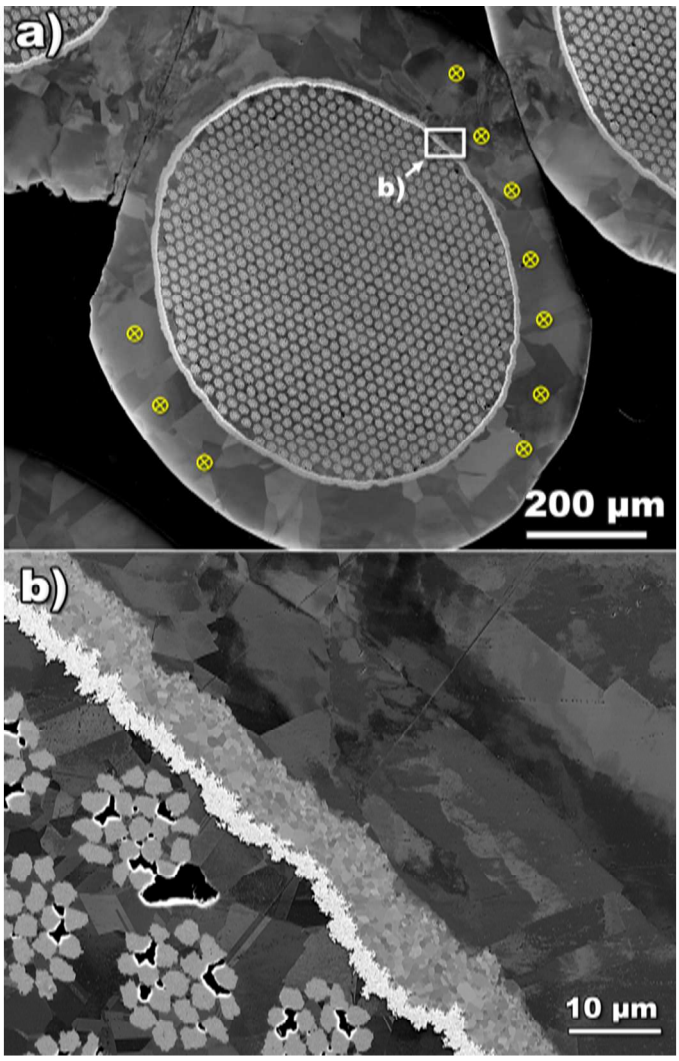

Figure 11. (a) FESEM standardless EDS measurements of local Sn and Cu content on the stabilization copper of a distorted strand in HFZ of the Short-BR sample. No Sn was found in any of these measurements. (b) The micro-misorientations seen in this back-scatter detector are evidence of cold work at the contact points of the strands. Notice that there is no cold work in the bronze beyond the diffusion barrier (non-Cu region).

Table 3, Table 4, Table 5 and Table 6 show the filament fracture counts for the HFZ of all samples following

the criterion in [10], with the exception that the short twist pitch samples are considered straight with curvatures higher than 0.95 rather than 0.98 (see glossary above). Notice the predominance of filament fractures in curved

Table 3. Crack count for extracted Baseline-BR strands

	HP bent	HP straight	LP bent	LP straight
a	0	0	1788	0
a	711	0	2168	13
b	0	0	469	21
b	4	0	255	23
a	0	0	648	0
a	0	0	841	0
c	0	0	0	0
c	0	0	54	0
d	0	0	1502	0
d	0	0	1326	137

Table 4. Crack count for extracted Baseline-IT strands.

	HP bent	HP straight	LP bent	LP straight
a	0	0	0	3
a	0	0	0	37
b	0	0	79	0
b	0	0	152	20
a	0	0	460	9
a	0	0	--	0
c	0	0	0	0
c	0	0	--	0
d	0	0	0	0
d	0	0	0	0

Table 5. Crack count for extracted Short-IT strands

	HP bent	HP straight	LP bent	LP straight
a	0	0	0	0
a	0	0	0	0
b	0	0	0	0
b	0	0	0	0
a	0	0	0	0
a	0	0	0	0
c	0	0	0	0
c	0	0	0	0
d	0	0	0	0
d	0	0	0	0

Table 6. Crack count for extracted Short-BR strands

	HP bent	HP straight	LP bent	LP straight
a	0	0	0	0
a	0	0	0	0
b	0	0	0	0
b	0	0	0	0
a	0	0	0	0
a	0	0	0	0
c	0	0	0	0
c	0	0	0	0
d	0	0	0	0
d	0	0	0	0

strands from the LP side on both baseline twist pitch samples. It should be noted that the absolute crack frequency from a Bronze Process strand cannot be directly compared to the crack numbers in an Internal Tin strand since there are more filaments in a Bronze Process strand and less current per filament (*i.e.* a crack across a filament in a Bronze Process strand is less detrimental than a crack in an Internal Tin strand). However, when the cracks per millimeter length of filament are calculated as in [8] the Baseline-BR has 80% more cracks per mm of filament than the Baseline-IT.

In all strands extracted from the baseline twist pitch samples, the filament fractures have a tensile morphology (see Figure 14 in [10]) indicating a predominance of bending, and relatively low contact stresses for reasons outlined in [10]. However, cold work could still be seen on the HP side of the baseline twist pitch samples without producing contact stress fractures. Figure 12 shows two interesting examples found on the HP side of the

Baseline-BR sample, in Figure 12c and Figure 12e one can see cold work produced by contact stresses with a neighboring strand—or perhaps the stainless steel components of the CICC. The cold work penetrates the bronze around the filaments and goes as deep as 200 μm into the non-copper area without producing filament fractures. But in Figure 12b and Figure 12d an absence of cold work is seen near the fracture region. The latter was the case in all LP strands of both the Baseline-IT and Baseline-BR suggesting high bending stresses and low contact stresses.

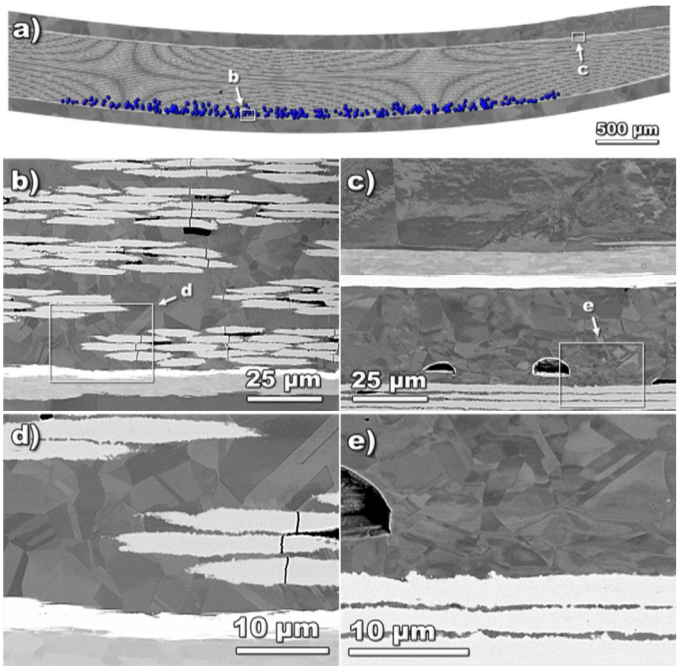

Figure 12. (a) Longitudinal cross-section of a strand extracted from the HP side of the HFZ of the Baseline-BR. Filament fractures are highlighted by blue markers. (b and d) Detail views of the filament fractures exhibiting a tensile morphology and no signs of cold work on the bronze around the filaments. (c and e) evidence of cold work reaching the non-copper area of the strands close to the contact point with a neighboring strand or the stainless steel components of the CICC.

The absence of cracks around the cold worked area of the Baseline-BR sample (as opposed to one of the samples studied in [10]) is consistent with the superior stability *in pinching* of the Bronze Process strands as modeled in [8] and measured in [13]. Nonetheless it is expected for the filaments around this cold work to have an enhanced compressive state and therefore suppressed transport properties.

Figure 13. Longitudinal cross sections of strands with similar high levels of curvature extracted from the HFZ of the (a) Short-BR sample and the (b) Short-IT sample; no filament fractures were observed in either cross-section.

Perhaps the most important finding of this study was the complete absence of filament fractures in the short

twist pitch samples. Figure 13 shows strands extracted from these samples having no filament factures. It should be noted that some cold-worked copper grains were observed on some strand-to-strand contact points in the high field zones of these short twist pitch samples. An example of this is shown in Figure 11. However, the absence of filament fractures (even in the IT strands, which are more prone to contact stresses [13]), and the fact that we found no evidence of this cold-work reaching the non-cu area—as we did for the baseline samples (see Figure 12), suggests a significant reduction in the contact stresses produced during electromagnetic operation of the short twist pitch samples as opposed to the baseline twist pitch samples. This could most likely be attributed to the increased contact area obtained during cabling.

C. *Experimental summary*

The most significant results of this study are:

1. The overall strand movement measured by strand center of mass offset was ~90 % lower in the short twist pitch conductors.
2. Filament fractures were completely suppressed in the short twist pitch samples.
3. The Internal Tin strands in the short twist pitch sample studied here exhibited a significant amount of barrier breakages that threaten the RRR of the strands.

IV. Discussion

A. *Introduction*

Below we will compare our results to those derived from other techniques in the literature to further illustrate the mechanical state of ITER CICCs after SULTAN testing.

B. *Strand movement, strain changes and T_{cs}*

The implied strand transverse movement from the offset measurements agrees with other deconstructions of baseline twist pitch SULTAN samples [3], [12] [22]. It was shown here that the accumulation of movement in baseline twist pitch conductors produces a void fraction expansion in the LP side and a void fraction compression in the HP side, both of which are *permanent*. In addition to this, irreversible effects such as filament fractures (on the LP side) and cold work in the bronze matrix (on the HP side) were found. All of the above are indications of a combination of high tensile *and* high compressive regions in the Nb_3Sn filament population developed during SULTAN testing. This result agrees with the broadening of the strain distributions measured by magnetic susceptibility [9] and neutron diffraction [23] on similar baseline twist pitch samples.

However, the transverse movement by itself does not explain the wide *shifting* of the peak strain values observed in [9]. Since the dominant stress component in a CICC is the compression imposed by the jacket [20], it could be argued that the *strain shift* has to do with longitudinal movement of the conductor which alleviates or enhances the average strain value—while on the other hand the *broadening* of the strain may be associated with transverse movement, hence the absence of broadening in the short twist pitch conductors in [24] and the absence of transverse movement in the short twist pitch conductors here.

With that said, there are two mechanisms that alter the strain state of a CICC in a SULTAN sample: transverse movement which broadens the tails of the strain distribution *and* longitudinal movement which shifts the average strain values. Devred *et. al.* [25] have suggested the possibility of *friction controlled jacket strain relaxation* and *cable softening* in SULTAN which are suspected to be artifacts of the SULTAN configuration and likely to be absent in a coil (where the magnetic field variations along the length are negligible compared to those in SULTAN). Therefore, the change in current sharing temperature, ΔT_{cs}, could be exacerbated by the introduction of jacket strain relaxation during SULTAN testing. This conclusion is supported by numerical simulations of baseline twist pitch CICC [16] where jacket slippage and cable softening is not taken into account and the shift of the strain peaks is much lower.

Looking for evidence of this suggested jacket slippage in the literature we found that variation in the jacket thermal compression is commonly seen when SULTAN samples are cut. It has been often found [3], [4], [23],

[26], [27] that there is more residual strain in the LFZ than the HFZ—suggesting relaxation of the strain imposed by the jacket around the HFZ—due to field gradients. In other words compression imposed by the jacket is alleviated in the HFZ, something that should be beneficial given the strain dependence of Nb_3Sn. This jacket strain relaxation and strain shift happens to all conductor designs. However, it was shown in [24] that baseline twist pitch conductors have a *negative* shift of the peak strain values, while short twist pitch conductors have a *positive* shift. Those observations raise a question: if there is strain relaxation (*i.e.* jacket slippage) on all samples, why are the baseline twist pitch samples not benefiting from it?

During our deconstructions it was observed that short twist pitch strands were heavily sintered together to a point where inter-strand slippage is *highly unlikely*, therefore it is safe to assume that any longitudinal movement (and thus average strain relaxation) comes from jacket slippage *only*—hence the beneficial shift seen in [24]. Then, in a real coil, having diminished or absent jacket slippage, a short twist pitch conductor should have minimal shifting of the average strain value and therefore the increase in T_{cs} (seen in SULTAN) should not be seen. A decrease in T_{cs} would also be unlikely, since the robustness of this conductor type will prevent any inter-strand slippage or transverse movement, thus preventing any broadening of the strain distributions.

However, in the case of baseline twist pitch conductors, the cycling of transverse movement may introduce longitudinal inter-strand slippage. This compound movement acts in one direction only (for each cycle) and may not return completely to its previous state, causing a slip-and-lock effect (ratcheting) which may explain the enhanced compressive state in baseline twist pitch conductors [24]. Consequently in a real coil, although the jacket strain relaxation is unlikely, a baseline twist pitch conductor still has the possibility of the slip-and-lock effect due to inter-strand slippage as a consequence of transverse movement which may still increase the average compressive strain state of the filaments and therefore the shift of the peak values may still be present.

C. *Strand distortion*

The difference in the distortion of Bronze Process strands compared to the distortion of Internal Tin strands in short twist pitch samples seen here agrees with that found by JAEA through destructive studies on unreacted short twist pitch conductors [7] (where sintering is absent because they have not been heat treated). Additionally, Takahashi *et. al.* [28] have investigated the I_c degradation of strands which have been indented prior to reaction in order to simulate the deformation found in short twist pitch conductors, and they see similar situations of barrier breakages as those seen here.

D. *A comment on overall void fraction*

One final parameter needs to be discussed, the overall void fraction. Although all conductors were designed to a target void fraction of 33%, Table 1 shows that the short twist pitch conductors have a slightly lower *measured* void fraction than the baseline twist pitch samples—this is most likely due to the deformation obtained during jacketing and compaction (which is hard to account for). Nonetheless one can't rule out that this decreased void fraction has no role on their outstanding performance. In fact, previous studies have shown better behavior during simulations [16] and tests [29] from other (much smaller) CICC with low void fractions between ~30% and ~32%. However, it should be noted that when comparing other ITER conductors with low void fractions such as the ITER conductor deconstructed in [12] (with a void fraction of ~29%), the conductor behavior is very similar to the Baseline-BR and Baseline-IT samples here. On the third part of this study we will explore a special conductor with similar behavior to the short twist pitch samples but having baseline twist pitch cabling stages. In that study, the conductor from [12] will be a crucial point of comparison and it will be revisited.

V. Conclusion

The short twist pitch cable design for the ITER Central Solenoid resolves the issue of electromagnetic degradation over extended Lorentz force cycling observed in SULTAN tests of ITER conductors. We have shown here that this is likely the result of significantly reduced transverse strand motion. It was observed that the short twist pitch sample using internal tin strands analyzed here exhibited some barrier breakages due to strand distortions produced during cabling. This issue was not seen for the short twist pitch sample using Bronze Process

strands. These conductors also developed significantly stronger strand sintering which was not broken during the extended SULTAN CS testing, as opposed to baseline twist pitch cables where such bond was broken during testing. The unbroken bond of the short twist pitch samples is consistent with the higher AC losses observed [30] and may be another compromise required by the short twist pitch for improved T_{cs} performance.

The baseline twist pitch conductors displayed significant transverse movement of strands which increases the local void fraction and reduces the strand-strand support on the LP side. This in turn allows some filament fractures to occur and in extreme cases this void fraction expansion can affect the HP side as well (Baseline-BR sample).

The above observations provide further explanation for the strain broadening found using magnetization measurements on similar baseline twist pitch SULTAN samples [9] and the lack of this broadening found in similar short twist pitch samples [24]. Magnetization measurements also show a *positive shift* in the peak strain values for short twist pitch conductors which may be linked to jacket strain relaxation given that these robust conductors behave as a single unit in every step of the deconstruction and inter-strand slippage is highly unlikely. On the other hand the magnetization measurements of baseline twist pitch conductors show a *negative shift* which may be linked to a stress accumulation due to a slip-and-lock mechanism during the inter-strand slippage enabled by the transverse movement.

The CS cable deconstructions in this study suggest that the most robust and stable conductor combines the short twist pitch design with the use of Bronze Process strands which are able to withstand the severe cabling deformations. This supports the choice made by the ITER organization of short twist pitch conductors for the Central Solenoid. However, a stiffer (post-heat treatment) strand (*i.e.* Internal Tin) has an advantage if longer twist pitches are desired to recover AC loss performance.

DISCLAIMER: The views and opinions expressed here do not necessarily reflect those of the ITER organization or the US Department of Energy.

Acknowledgments

Special thanks are given to Nicolai Martovetsky (ITER USIPO), Matthew Jewell (formerly of ITER-IO, now at UW Eau-Claire) and Ian Pong (formerly of ITER-IO, now at LBNL) for fruitful discussions. The CICCs were provided by courtesy of Pierluigi Bruzzone (CFRP Villigen, CH) with agreement from the Japan Atomic Energy Agency (JAEA) and ITER USIPO. This work was supported by the ITER-IO under purchase order ITER/CT/11/4300000511, ITER USIPO under contract 6400011187, and the US Department of Energy Office of Fusion Energy Sciences under award DE-FG02-06ER54881. The National High Magnetic Field Laboratory where the experiments were performed is supported by the National Science Foundation Cooperative Agreement DMR-1157490 and by the State of Florida.

References

[1] M. Breschi, A. Devred, M. Casali, D. Bessette, M. C. Jewell, N. Mitchell, I. Pong, A. Vostner, P. Bruzzone, B. Stepanov, T. Boutboul, N. Martovetsky, K. Kim, Y. Takahashi, V. Tronza, and W. Yu, "Results of the TF conductor performance qualification samples for the ITER project," *Supercond. Sci. Technol.*, vol. 25, no. 9, p. 095004, Sep. 2012.

[2] A. Devred, I. Backbier, D. Bessette, G. Bevillard, M. Gardner, M. Jewell, N. Mitchell, I. Pong, and A. Vostner, "Status of ITER Conductor Development and Production," *IEEE Trans. Appl. Supercond.*, vol. 22, no. 3, pp. 4804909–4804909, 2012.

[3] T. Hemmi, Y. Nunoya, Y. Nabara, M. Yoshikawa, K. Matsui, H. Kajitani, K. Hamada, T. Isono, Y. Takahashi, N. Koizumi, H. Nakajima, B. Stepanov, and P. Bruzzone, "Test Results and Investigation of T_{cs} Degradation in Japanese ITER CS Conductor Samples," *IEEE Trans. Appl. Supercond.*, vol. 22, no. 3, pp. 4803305–4803305, 2012.

[4] A. Devred, D. Bessette, P. Bruzzone, K. Hamada, T. Isono, N. Martovetsky, N. Mitchell, Y. Nunoya, K. Okuno, I. Pong, W. Reiersen, C. M. Rey, B. Stepanov, Y. Takahashi, and A. Vostner, "Status of Conductor

Qualification for the ITER Central Solenoid," *IEEE Trans. Appl. Supercond.*, vol. 23, no. 3, pp. 6001208–6001208, Jun. 2013.

[5] P. Libeyre, N. Mitchell, D. Bessette, Y. Gribov, C. Jong, and C. Lyraud, "Detailed design of the ITER central solenoid," *Fusion Eng. Des.*, vol. 84, no. 7–11, pp. 1188–1191, Jun. 2009.

[6] P. Bruzzone, B. Stepanov, R. Wesche, E. Salpietro, A. Vostner, K. Okuno, T. Isono, Y. Takahashi, H. C. Kim, K. Kim, A. K. Shikov, and V. E. Sytnikov, "Results of a New Generation of ITER TF Conductor Samples in SULTAN," *IEEE Trans. Appl. Supercond.*, vol. 18, no. 2, pp. 459–462, 2008.

[7] A. Devred, I. Backbier, D. Bessette, G. Bevillard, M. Gardner, C. Jong, F. Lillaz, N. Mitchell, G. Romano, and A. Vostner, "Challenges and status of ITER conductor production," *Supercond. Sci. Technol.*, vol. 27, no. 4, p. 044001, Apr. 2014.

[8] N. Mitchell, A. Devred, D. C. Larbalestier, P. J. Lee, C. Sanabria, and A. Nijhuis, "Reversible and irreversible mechanical effects in real cable-in-conduit conductors," *Supercond. Sci. Technol.*, vol. 26, no. 11, p. 114004, Nov. 2013.

[9] C. Calzolaio, P. Bruzzone, and B. Stepanov, "Monitoring of the Thermal Strain Distribution in CICCs During the Cyclic Loading Tests in SULTAN," *IEEE Trans. Appl. Supercond.*, vol. 23, no. 3, pp. 4200404–4200404, 2013.

[10] C. Sanabria, P. J. Lee, W. Starch, T. Blum, A. Devred, M. C. Jewell, I. Pong, N. Martovetsky, and D. C. Larbalestier, "Metallographic autopsies of full-scale ITER prototype cable-in-conduit conductors after full testing in SULTAN: 1. The mechanical role of copper strands in a CICC," *Supercond. Sci. Technol.*, vol. 28, no. 8, p. 085005, Aug. 2015.

[11] J. W. Ekin, "Strain Effects in Superconducting Compounds," in *Advances in Cryogenic Engineering Materials*, A. F. Clark and R. P. Reed, Eds. Springer US, 1984, pp. 823–836.

[12] C. Sanabria, P. J. Lee, W. Starch, I. Pong, A. Vostner, M. C. Jewell, A. Devred, and D. C. Larbalestier, "Evidence that filament fracture occurs in an ITER toroidal field conductor after cyclic Lorentz force loading in SULTAN," *Supercond. Sci. Technol.*, vol. 25, no. 7, p. 075007, Jul. 2012.

[13] A. Nijhuis, R. P. P. van Meerdervoort, H. J. G. Krooshoop, W. a. J. Wessel, C. Zhou, G. Rolando, C. Sanabria, P. J. Lee, D. C. Larbalestier, A. Devred, A. Vostner, N. Mitchell, Y. Takahashi, Y. Nabara, T. Boutboul, V. Tronza, S.-H. Park, and W. Yu, "The effect of axial and transverse loading on the transport properties of ITER Nb_3Sn strands," *Supercond. Sci. Technol.*, vol. 26, no. 8, p. 084004, Aug. 2013.

[14] P. Bruzzone, B. Stepanov, R. Wesche, A. della Corte, L. Affinito, M. Napolitano, and A. Vostner, "Test Results of a Cable-in-Conduit Conductor With Variable Pitch Sequence," *IEEE Trans. Appl. Supercond.*, vol. 19, no. 3, pp. 1448–1451, Jun. 2009.

[15] K. Hamada, H. Nakajima, K. Matsui, K. Kawano, K. Takano, F. Tsutsumi, K. Okuno, O. Teshima, and K. Soejima, "Development of Jacketing Technologies for Iter CS and TF Conductor," presented at the Advances in Cryogenic Engineering Materials, 2008, vol. 986, pp. 76–83.

[16] H. Bajas, D. Durville, D. Ciazynski, and A. Devred, "Numerical Simulation of the Mechanical Behavior of ITER Cable-In-Conduit Conductors," *IEEE Trans. Appl. Supercond.*, vol. 20, no. 3, pp. 1467–1470, 2010.

[17] J. Schindelin, I. Arganda-Carreras, E. Frise, V. Kaynig, M. Longair, T. Pietzsch, S. Preibisch, C. Rueden, S. Saalfeld, B. Schmid, J.-Y. Tinevez, D. J. White, V. Hartenstein, K. Eliceiri, P. Tomancak, and A. Cardona, "Fiji: an open-source platform for biological-image analysis," *Nat. Methods*, vol. 9, no. 7, pp. 676–682, Jul. 2012.

[18] C. A. Schneider, W. S. Rasband, and K. W. Eliceiri, "NIH Image to ImageJ: 25 years of image analysis," *Nat. Methods*, vol. 9, no. 7, pp. 671–675, Jul. 2012.

[19] A. Nijhuis and Y. Ilyin, "Transverse load optimization in Nb_3Sn CICC design; influence of cabling, void fraction and strand stiffness," *Supercond. Sci. Technol.*, vol. 19, no. 9, p. 945, Sep. 2006.

[20] N. Mitchell, "Finite element simulations of elasto-plastic processes in Nb_3Sn strands," *Cryogenics*, vol. 45, no. 7, pp. 501–515, Jul. 2005.

[21] F. R. Fickett, *Standards for measurement of the critical fields of superconductors*. National Bureau of Standards, 1985.

[22] K. Matsui, T. Isono, Y. Nunoya, T. Hemmi, Y. Okui, M. Oshikiri, N. Koizumi, Y. Takahashi, K. Okuno, B. Stepanov, and P. Bruzzone, "Test Results of the Third Japanese SULTAN Sample," *IEEE Trans. Appl. Supercond.*, vol. 19, no. 3, pp. 1470–1473, 2009.

[23] T. Hemmi, S. Harjo, Y. Nunoya, H. Kajitani, N. Koizumi, K. Aizawa, S. Machiya, and K. Osamura, "Neutron diffraction measurement of internal strain in the first Japanese ITER CS conductor sample," *Supercond. Sci. Technol.*, vol. 26, no. 8, p. 084002, Aug. 2013.

[24] C. Calzolaio and P. Bruzzone, "Analysis of the CICCs performance through the measurement of the thermal strain distribution of the Nb_3Sn filaments in the cable cross section," *IEEE Trans. Appl. Supercond.*, vol. Early Access Online, 2013.

[25] A. Devred, C. Jong, and N. Mitchell, "Strain redistribution effects on current-sharing measurements on straight samples of large Nb_3Sn cable-in-conduit conductors," *Supercond. Sci. Technol.*, vol. 25, no. 5, p. 054009, May 2012.

[26] Y. Nabara, Y. Nunoya, T. Isono, K. Hamada, Y. Takahashi, K. Matsui, T. Hemmi, K. Kawano, N. Koizumi, N. Ebisawa, M. Iguchi, H. Kajitani, M. Oshikiri, Y. Uno, F. Tsutsumi, M. Yoshikawa, H. Nakajima, K. Okuno, P. Bruzzone, and B. Stepanov, "Examination of Japanese Mass-Produced Conductors for ITER Toroidal Field Coils," *IEEE Trans. Appl. Supercond.*, vol. 22, no. 3, pp. 4804804–4804804, Jun. 2012.

[27] S. A. March, P. Bruzzone, B. Stepanov, D. Bessette, T. Boutboul, A. Devred, N. Mitchell, P. Readman, and A. Vostner, "Results of the TFEU6 Sample Tested in SULTAN," *IEEE Trans. Appl. Supercond.*, vol. 23, no. 3, pp. 4200204–4200204, 2013.

[28] Y. Takahashi, Y. Nabara, H. Ozeki, T. Hemmi, Y. Nunoya, T. Isono, K. Matsui, K. Kawano, M. Oshikiri, Y. Uno, F. Tsutsumi, K. Shibutani, T. Kawasaki, K. Okuno, Y. Murakami, M. Tani, G. Sato, Y. Nakata, and M. Sugimoto, "Cabling Technology of Conductor for ITER Central Solenoid," *IEEE Trans. Appl. Supercond.*, vol. 24, no. 3, pp. 1–4, Jun. 2014.

[29] A. Vostner, P. Bauer, R. Wesche, U. Besi Vetrella, B. Stepanov, A. della Corte, A. Portone, E. Salpietro, and P. Bruzzone, "Development of the EFDA Dipole High Field Conductor," *IEEE Trans. Appl. Supercond.*, vol. 18, no. 2, pp. 544–547, Jun. 2008.

[30] Y. Nabara, T. Hemmi, H. Kajitani, H. Ozeki, T. Suwa, M. Iguchi, Y. Nunoya, T. Isono, K. Matsui, N. Koizumi, F. Tsutsumi, Y. Uno, M. Oshikiri, K. Shibutani, Y. Takahashi, K. Okuno, Y. Murakami, T. Miyatake, M. Sugimoto, A. Takagi, Y. Nakada, K. Miyashita, K. Sedlak, B. Stepanov, and P. Bruzzone, "Impact of Cable Twist Pitch on Degradation and AC Loss in Conductors for ITER Central Solenoids," *IEEE Trans. Appl. Supercond.*, vol. 24, no. 3, pp. 1–5, Jun. 2014.